J Electroceram (2009) 22:436–441
DOI 10.1007/s10832-008-9489-z

# Ni–Mn–Fe–Cr–O negative temperature coefficient thermistor compositions: Correlation between processing conditions and electrical characteristics

**Justin M. Varghese · A. Seema · K. R. Dayas**

Received: 25 September 2007 / Accepted: 18 March 2008 / Published online: 15 April 2008
© Springer Science + Business Media, LLC 2008

**Abstract** A study has been carried out to correlate the effect of sintering temperature on the microstructural, electrical and reliability aspects of $Ni_{0.75}Mn_{(2.25-x-y)}Cr_xFe_yO_4$ ($x$=0 to 0.3 and $y$=0 to 0.3) negative temperature coefficient thermistor compositions prepared by solid-state route. The calcined and sintered compositions were characterized by X-ray diffraction and Scanning Electron Microscopy. The existence of cubic spinel single-phase region was determined by sintering $Ni_{0.75}Mn_{(2.25-x-y)}Cr_xFe_yO_4$ samples in air at temperatures 1150 to 1250 °C. X-ray diffraction patterns of samples sintered above 1200 °C shows additional Bragg reflections of a rock salt structured NiO phase besides normal cubic spinel. A maximum $B$-value of 4044 K was obtained for $Ni_{0.75}Mn_{1.95}Cr_{0.25}$ $Fe_{0.05}O_4$ composition at a sintering temperature 1250 °C/3 h. The reliability of the thermistor compositions were evaluated by performing accelerated ageing based on thermal cycling test. We found that chromium enhances the reliability of $Ni_{0.75}Mn_{(2.25-x-y)}Cr_xFe_yO_4$ ($x$=0 to 0.3 and $y$=0 to 0.3) based NTC thermistor compositions. A maximum reliability of +0.25% resistance drift was observed at sintering temperature 1200 °C for 0.25 mol% chromium content. Excellent reliability of $Ni_{0.75}Mn_{(2.25-x-y)}Cr_xFe_yO_4$ NTC thermistor compositions makes it ideal candidates for high-performance thermal sensor applications.

**Keywords** Nickel manganite · NTC thermistors · Sintering temperature · Electrical properties

J. M. Varghese · A. Seema (✉) · K. R. Dayas
Centre for Materials for Electronics Technology (C-MET), Thrissur, Kerala, India, PIN 680 771
e-mail: seemaansari@yahoo.com

## 1 Introduction

Nickel manganite ($NiMn_2O_4$) based negative temperature coefficient (NTC) thermistor compositions are extensively used for the development of thermal sensors. These materials exhibit a monotonic decrease in electrical resistance with increase in temperature. Ternary or quaternary oxide solid solutions based on transition metals (e.g. Mn, Ni, Co, Fe, Cu, Ti, etc.) are generally employed for the synthesis of NTC ceramics. The wide spectrum of applications alone should make NTC thermistors a highly desirable component for temperature control, circuit compensation and precise monitoring, particularly in automobiles, aerospace and cryogenic applications [1–5].

By varying the types of oxides used, their relative proportions, and the processing conditions, a wide range of resistivity and temperature coefficient characteristics can be obtained [6–13]. The main characteristics of NTC thermistors are their specific resistivity, material constant (B-value) and temperature coefficient of resistance.

To meet the stringent requirements of new generation NTC thermal sensors, a greater emphasis should be given to enhance the device stability and performance. Since 1950s Ni–Mn–O based ternary or quaternary transition metal oxide systems are generally used for NTC thermistor manufacturing [7–13]. The composition range of these systems is often quite narrow, so to extend it the compound is usually doped with impurities. Dopants facilitate controlled valence semi conduction or dilution by which the conductivity can be adjusted. Recently we have reported the modification of Ni–Mn–O compositions by the addition of $Cr_2O_3$ and $Fe_2O_3$ [14]. The present study focusing on the development of a reliable NTC material composition based on Ni–Mn–Fe–Cr–O system. In particular, we reports the effect of calcination and sintering

**Table 1** Molar compositions of samples prepared.

| Sample code | Composition (mol) | | | |
|---|---|---|---|---|
| | Ni | Mn | Cr | Fe |
| $A_1$ | 0.75 | 2.25 | 0 | 0 |
| $A_2$ | 0.75 | 2.20 | 0 | 0.05 |
| $A_3$ | 0.75 | 2.15 | 0.05 | 0.05 |
| $A_4$ | 0.75 | 2.10 | 0.1 | 0.05 |
| $A_5$ | 0.75 | 2.05 | 0.15 | 0.05 |
| $A_6$ | 0.75 | 2.00 | 0.2 | 0.05 |
| $A_7$ | 0.75 | 1.95 | 0.25 | 0.05 |
| $A_8$ | 0.75 | 1.95 | 0.3 | 0 |
| $A_9$ | 0.75 | 1.95 | 0 | 0.3 |

temperature on the microstructure and electrical characteristics of $Ni_{0.75}Mn_{(2.25-x-y)}Cr_xFe_yO_4$ ($x$=0.05 to 0.25 and $y$= 0.05) NTC thermistor compositions. The reliability of the material is of prime importance in the development of NTC thermistors. As a measure of stability of rated properties, the reliability studies of the thermistor compositions were also conducted.

## 2 Experimental procedures

From the phase diagram of Ni–Mn–O system [15] we have selected $Ni_{0.75}Mn_{2.25}O_4$ system having a $^{Ni}/_{(Ni+Mn)}$ ratio 0.25 as the basic composition for the development of $Ni_{0.75}Mn_{(2.25-x-y)}Cr_xFe_yO_4$ NTC thermistor materials. In the present investigation 9 different compositions were prepared based on $Ni_{0.75}Mn_{(2.25-x-y)}Cr_xFe_yO_4$ ($x$=0 to 0.3 and $y$=0, 0.05, 0.3) system as given in Table 1.

All the material compositions were synthesized through solid-state route. For getting higher quality, close-tolerance and good reproducibility over lots, high purity raw materials; manganese carbonate, nickel carbonate basic hydrate ($NiCO_3$ $2Ni(OH)_2$ $xH_2O$), $Cr_2O_3$ and $Fe_2O_3$ (Sigma-Aldrich, USA), of +99% purity were used. The raw materials were accurately weighed, transferred to polypropylene jars and ball milled for 24 h to get a uniform mix. Thermal analysis of the composition mix was carried out by Thermo gravimetric/Differential thermal analysis (Perkin Elmer, Diamond TG/DTA, USA) at a heating rate of 10 °C per minute in oxygen atmosphere. To optimize the calcination condition, the raw materials were calcined at 700–900 °C for 3 h. The calcined powder was ball milled for 48 h to achieve well-controlled uniform crystallite size, required for better chemical homogeneity and better sinterability. The mix was then sieved (400 mesh size) and dried. 5% PVA solution was used for granulation of fine calcined powder. The green compacts were formed by uniaxial compaction of the granulated powder to a size of 6 mm diameter and 1.2 mm thick discs. The green compacts were sintered at 1150 °C, 1200 °C, and 1250 °C for 3 h in air and slowly cooled.

The phase purity of the calcined and sintered compositions were studied using XRD (Bruker AXS D5005, Germany) at a scanning rate of 0.25 degree per minute. The microstructural features of the calcined and sintered compositions were analyzed using Scanning Electron Microscopy (Philips XL-30 SEM). For electrical characterization, the sintered discs were electroded using a thermistor grade silver paste and annealed at 750 °C for 30 min in a belt furnace. Electrical resistance was measured, between 25 °C and 85 °C in steps of 5 °C in a constant temperature

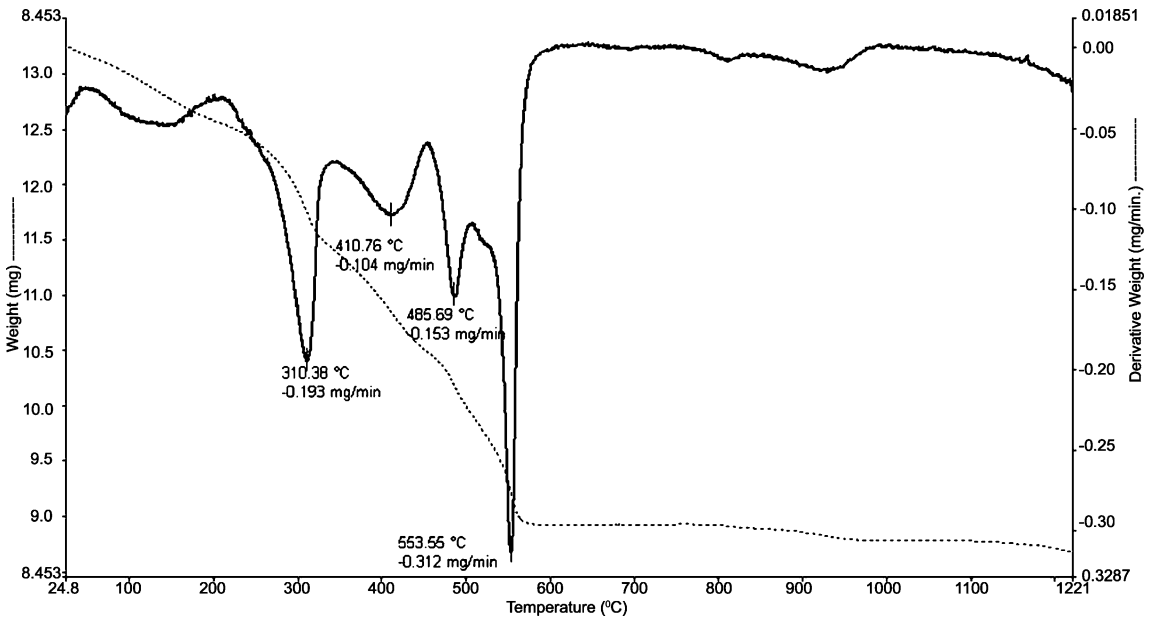


**Fig. 1** TG/DTA curve of the composition $Ni_{0.75}Mn_{2.00}Cr_{0.2}Fe_{0.05}O_4$

silicone oil bath (Model 7320, Hart Scientific, USA) with a temperature uniformity±0.005 °C, using a precise digital multimeter (Fluke 45 Dual display, USA) with 0.05% dc current accuracy.

To complement the reliability study of Ni–Mn–Fe–Cr–O NTC compositions, a thermal cycling experiment based on accelerated testing schemes were performed on the NTC thermistor samples. For this process, first the discs with leads were aged in air oven for 7 days at 150 °C. After this, the discs were kept in a programmable automated chamber that has two compartments maintained at -40 °C and 155 °C. The test was performed by the rapid change of temperature cycle; −40 °C and 155 °C. 100 cycles were repeated with an exposure time of 18 s at each temperature. After 1 h the resistance measurements were again repeated and the resistance drift ($\Delta R$) calculated.

## 3 Results and discussions

The TG/DTA curve of composition $A_6$ is given in Fig. 1. A total weight loss of approximately 35% was observed. The weight losses at 310 °C, 410 °C, and 485 °C are associated with the removal of water of crystallization, decarboxylation and removal of hydroxyl group (from Nickel carbonate basic hydrate) respectively. The loss at 553 °C is attributed to the decarboxylation of $MnCO_3$ [16–17].

Particle size and its distribution greatly affect the physical properties of powders, such as packing density, grain porosity and firing range [18]. SEM image (Fig. 2) of calcined powder ($A_5$) particles having uniform size distribution. The calcined powder (48 h ball milled) shows an average particle size of around 1 μm with a narrow particle-size distribution.

Figure 3 illustrates the XRD patterns of powders ($A_5$) calcined at 700 °C to 900 °C, which indicates a single-phase cubic spinel formation at 800 °C. A secondary phase of NiO

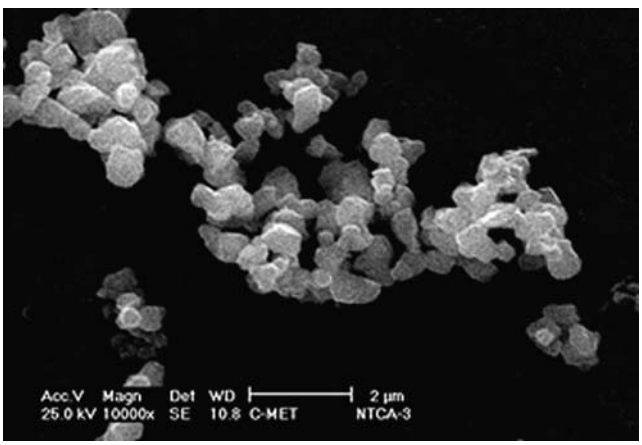


**Fig. 2** SEM image of powder of $Ni_{0.75}Mn_{2.05}Cr_{0.15}Fe_{0.05}O_4$ composition calcined at 800 °C

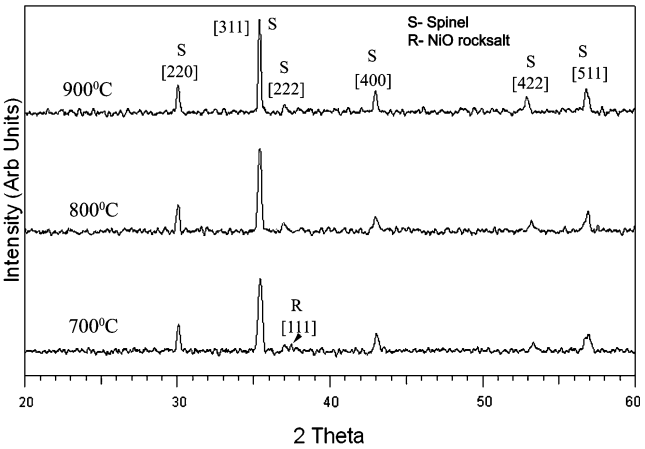


**Fig. 3** XRD patterns of powder of $Ni_{0.75}Mn_{2.05}Cr_{0.15}Fe_{0.05}O_4$ composition calcined at 700 °C, 800 °C and 900 °C

with rock salt structure was observed at lower calcination temperatures (700 °C), which indicates incompletion of calcination reaction. Thus a calcination temperature of 800 °C was optimized for the system of $Ni_{0.75}Mn_{(2.25-x-y)}Cr_xFe_yO_4$ for which further sintering studies were done. For Ni–Mn–O system (with a $^{Ni}/_{(Ni+Mn)}$ ratio 0.25 to 0.28) the spinel formation starts at 700 °C [15].

Many factors are believed to affect the final characteristics of NTC thermistors, among which the effect due to sintering temperature and cooling rate is of prime importance [10–13, 20–21]. In this study a cooling rate of 2 °C per minute applied after sintering. All the sintered compacts show a linear shrinkage of 15–19%. The experimental density was found to be 96–98% of the theoretical density. Figure 4 depicts the XRD patterns of $Ni_{0.75}Mn_{(2.25-x-y)}Cr_xFe_yO_4$ compositions sintered at 1150 °C, 1200 °C and 1250 °C. It reveals that the cubic spinel structure (space group Fd $3m$) is retained even after the addition of $Cr_2O_3$ for all the compositions sintered at 1150–1200 °C. An interesting observation is that the decomposition temperature region of cubic spinel $Ni_{0.75}Mn_{(2.25-x-y)}Cr_xFe_yO_4$ compositions is found to be higher (1150 to 1200 °C) compared to the

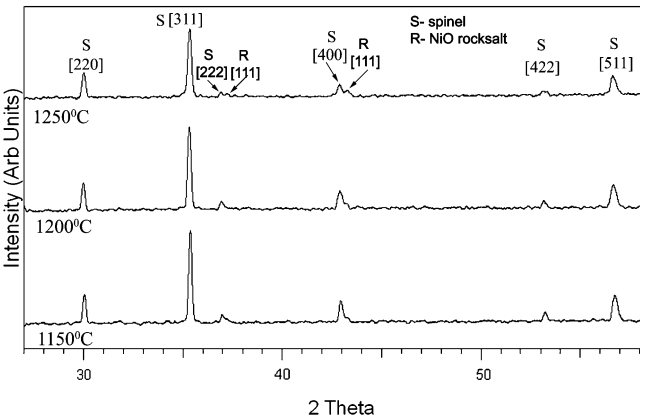


**Fig. 4** XRD patterns of powder of $Ni_{0.75}Mn_{2.05}Cr_{0.15}Fe_{0.05}O_4$ composition sintered at 1150 °C, 1200 °C and 1250 °C

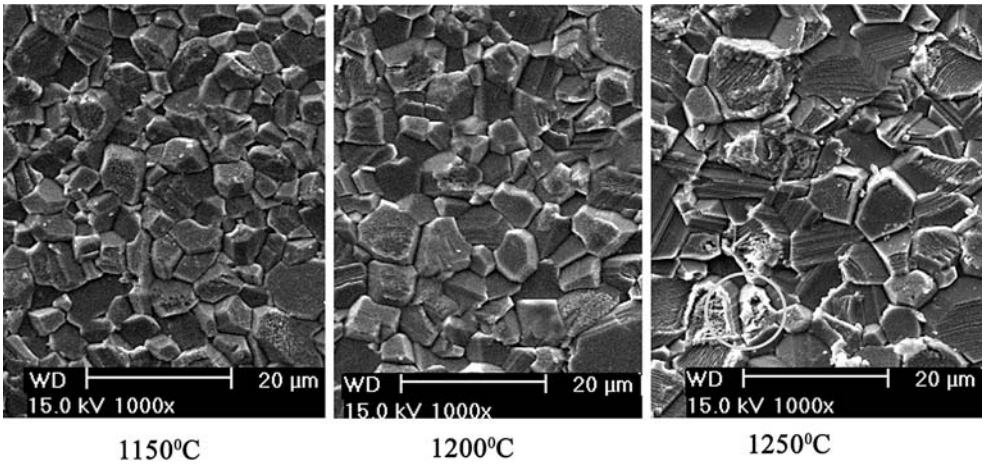


**Fig. 5** SEM photographs of surface of $Ni_{0.75}Mn_{2.05}Cr_{0.15}Fe_{0.05}O_4$ ceramic discs at different sintering temperatures

Ni–Mn–O counterparts (with a $^{Ni}/_{(Ni+Mn)}$ ratio 0.25 to 0.28), a decomposition temperature region of 1000 to 1050 °C was observed in the latter case [15]. NTC compositions that have been slowly cooled after sintering are found to be single-phase and free from lattice defects such as dislocations or planar defects [5,7]. Previous studies on Cr-substituted $Mn_{1.1}Ni_{1.4}Co_{0.5-x}Cr_xO_4$ showed single phase cubic spinel Mn–Ni–Co–Cr oxide formation, suggesting that the substituted Cr suppressed a loss and transportation of oxygen [13]. The formation of monophase cubic spinel is considered to be very important for the development of stable and reliable NTC thermistor compositions.

As the sintering temperature is raised to above 1200 °C, partial decomposition of cubic spinel occurs with the formation of rock salt NiO phase. XRD shows an increase in the relative intensity of the rock salt structured NiO phase reflection besides cubic spinel at a sintering temperature of 1250 °C (Fig. 4). Thus the spinel will become Mn rich compared to the bulk. In addition a small broadening of [311] spinel reflection was observed at 1250 °C, which is an indication of onset of tetragonal distortion found in Mn rich spinels [19–20]. The results were further confirmed by SEM analysis of samples sintered at different temperatures (Fig. 5), which indicates a second phase formation at 1250 °C (indicated in circle in SEM picture). Moreover, non-uniform grains were observed at higher sintering temperatures particularly at 1250 °C.

SEM micrographs of samples sintered at 1150 °C and 1200 °C shows uniform polycrystalline single phase spinel formation, while at 1250 °C the appearance of secondary phase was noticed with non-uniform grain size. As usual an increase in grain size was observed with increase in sintering temperature. Gyorgyfalva et al. suggests that with the increase of sintering temperature, $Mn^{3+}$clustering will occur and the surrounding matrix becomes increasingly NiO rich [20–21].

Studies shows that the segregation occurs as a result of the stresses developed due to the different thermal expansion coefficients of the contributing species. Also the heat of solution of many solutes in oxide systems is high, as a result segregation of solutes in the vicinity of grain boundary is often observed, particularly in samples that are slowly cooled [21, 22]. Also the size of the segregating cation is a dominant factor in segregation, the

**Table 2** Electrical characteristics of $Ni_{0.75}Mn_{(2.25-x-y)}Cr_xFe_yO_4$ compositions at different sintering temperatures.

| Sintering temperature (°C) | Sample code | $B_{25/85}$ | Resistivity at 25 °C, $\rho_{25}$ (Ω cm) | Temperature coefficient of resistance, ($\alpha$) |
|---|---|---|---|---|
| 1150 | $A_1$ | 3,889 | 1,757 | −0.0437 |
| | $A_2$ | 3,908 | 1,850 | −0.0440 |
| | $A_3$ | 3,903 | 2,116 | −0.0439 |
| | $A_4$ | 3,919 | 2,292 | −0.0441 |
| | $A_5$ | 3,933 | 2,415 | −0.0442 |
| | $A_6$ | 3,943 | 2,778 | −0.0444 |
| | $A_7$ | 3,954 | 3,118 | −0.0445 |
| | $A_8$ | 3,937 | 3,179 | −0.0443 |
| | $A_9$ | 3,852 | 2,596 | −0.0433 |
| 1200 | $A_1$ | 3,902 | 1,793 | −0.0439 |
| | $A_2$ | 3,928 | 1,957 | −0.0442 |
| | $A_3$ | 3,931 | 2,291 | −0.0443 |
| | $A_4$ | 3,951 | 2,431 | −0.0445 |
| | $A_5$ | 3,989 | 2,912 | −0.0449 |
| | $A_6$ | 4,002 | 3,108 | −0.0450 |
| | $A_7$ | 4,012 | 3,302 | −0.0451 |
| | $A_8$ | 3,966 | 2,969 | −0.0446 |
| | $A_9$ | 3,872 | 3,117 | −0.0436 |
| 1250 | $A_1$ | 3,912 | 2,040 | −0.0440 |
| | $A_2$ | 3,937 | 2,129 | −0.0443 |
| | $A_3$ | 3,961 | 2,359 | −0.0446 |
| | $A_4$ | 3,986 | 2,626 | −0.0448 |
| | $A_5$ | 4,020 | 3,120 | −0.0452 |
| | $A_6$ | 4,032 | 3,385 | −0.0454 |
| | $A_7$ | 4,044 | 3,570 | −0.0455 |
| | $A_8$ | 3,988 | – | −0.0440 |
| | $A_9$ | 3,884 | – | −0.0443 |

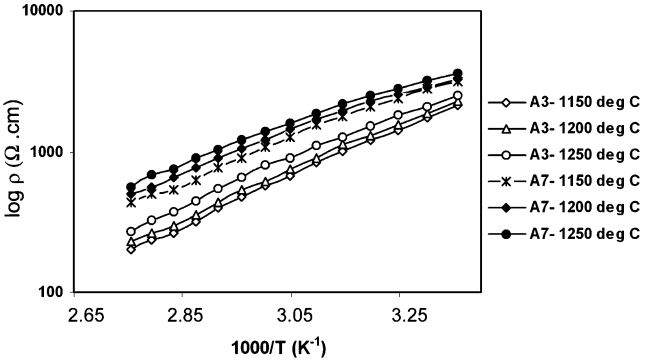


**Fig. 6** Relationship between log $\rho$ and reciprocal of the absolute temperature ($1/T$) for $Ni_{0.75}Mn_{(2.25-x-y)}Cr_xFe_yO_4$ ceramics at different sintering temperatures

larger the size the stronger will be the enrichment at the surface. Here $Ni^{2+}$is the largest ion compared to the other contributing cations, so the segregation results in the formation of NiO as the second phase [6].

In nickel manganite spinels the semiconduction is satisfactorily described by a hopping process of charge carriers between $Mn^{3+}$and $Mn^{4+}$on octahedral sites via localized states. The two main electrical parameters derived from resistance-temperature characteristics, material constant ($B$-value) and temperature coefficient of resistance-TCR ($\alpha$) determine the condition under which a given thermistor material may be utilized [1, 2].

The resistance ($R$)-temperature ($T$) relationship of an NTC thermistor can be represented as

$$R = Ae^{(B/T)} \tag{1}$$

Where '$B$' is the material constant ($B$-value) and '$A$' is a constant related to device dimensions and resistivity ($\rho$). $B$-value is simply '$q/k$' where '$q$' is the activation energy for the hopping process and '$k$' is Boltzmann's constant. $B$-value is usually calculated using the relation

$$B_{25/85} = \frac{T_{25}T_{85}\ln(R_{25}/R_{85})}{T_{85}-T_{25}} \tag{2}$$

where $R_{25}$ and $R_{85}$ are the resistance values at temperature 25 °C ($T_{25}$) and 85 °C ($T_{85}$) respectively. Another parameter TCR or $\alpha$ is defined as the rate of change of resistance ($R$) with temperature ($T$) to the resistance at a specified temperature and is given by expression,

$$\alpha_{25} = (1/R)\mathrm{d}R/\mathrm{d}T = -B/T^2 \tag{3}$$

The main electrical characteristics of the compositions are listed in Table 2. Figure 6 shows a linear dependence of log $\rho$ versus $1/T$ over a wide temperature and compositional range, an indication of good NTC thermistor characteristic [1–4]. The result shows an increase in activation energy, resistivity and hence $B$-value with increase in sintering temperature. The increase in resistance may be attributed to the change in cation distribution in the sublattice of the spinel phase [8]. The variations in hopping site concentration, hopping distance and hopping probability greatly affect the electrical characteristics of NTC thermistors. The cationic distribution in nickel manganite is sensitive to the cooling rate after the sintering process [5], a decrease in degree of inversion ($\lambda$) was generally observed on heating [21]. In NTC thermistors, electrical response to temperature depends mainly on the manner in which hoping charge carriers are generated and the manner in which they move. As explained, $Mn^{3+}$clustering in octahedral sites of spinel increases with increase in sintering temperature, which results in a decrease of hopping

**Table 3** Reliability results of $Ni_{0.75}Mn_{(2.25-x-y)}Cr_xFe_yO_4$ compositions at various sintering temperatures.

| Sintering temperature (°C) | Sample code | Initial reading (Ω) | | After test (Ω) | | Resistance drift ($\Delta R$) after test (%) | |
|---|---|---|---|---|---|---|---|
| | | $R_{25}$ | $R_{85}$ | $R_{25}$ | $R_{85}$ | $R_{25}$ | $R_{85}$ |
| 1150 | $A_1$ | 478.32 | 53.68 | 485.25 | 54.54 | 1.45 | 1.61 |
| | $A_3$ | 501.29 | 55.82 | 503.89 | 56.14 | 0.52 | 0.58 |
| | $A_5$ | 519.25 | 56.85 | 521.22 | 57.12 | 0.38 | 0.48 |
| | $A_7$ | 587.72 | 63.59 | 589.77 | 63.85 | 0.35 | 0.41 |
| 1200 | $A_1$ | 491.54 | 54.75 | 498.32 | 55.58 | 1.38 | 1.53 |
| | $A_3$ | 513.21 | 56.23 | 515.72 | 56.53 | 0.49 | 0.54 |
| | $A_5$ | 581.3 | 61.67 | 583.21 | 61.94 | 0.33 | 0.45 |
| | $A_7$ | 619.33 | 64.86 | 620.87 | 65.08 | 0.25 | 0.34 |
| 1250 | $A_1$ | 504.53 | 55.93 | 509.23 | 56.45 | 1.51 | 1.58 |
| | $A_3$ | 531.17 | 57.27 | 532.18 | 57.38 | 0.53 | 0.59 |
| | $A_5$ | 634.26 | 66.18 | 634.26 | 66.18 | 0.28 | 0.36 |
| | $A_7$ | 661.40 | 68.01 | 661.40 | 68.01 | 0.43 | 0.40 |
| | $A_8$ | 1,554.0 | 165.29 | 1,566.1 | 166.50 | 0.73 | 0.74 |
| | $A_9$ | 1,360.0 | 153.36 | 1,373.0 | 154.44 | 1.10 | 1.15 |

frequency between $Mn^{3+}$and $Mn^{4+}$. This effect ultimately leads to an increased resistance.

Our previous studies [14] shows a valence state of 3+ for chromium and iron in $Ni_{0.75}Mn_{(2.25-x-y)}Cr_xFe_yO_4$ system, also both ions occupies the octahedral sites of the cubic spinel. According to dilution principle, $Fe^{3+}$and $Cr^{3+}$ substitution does not change the valence of $Mn^{3+}$, it changes only the hopping distance between the charge carriers $Mn^{3+}/Mn^{4+}$ [23–24]. Consequently the hopping probability of charge transfer decreases with increase in Cr and Fe content. The results (Table 2) show a greater effect of chromium than iron on the electrical characteristics of Ni-Mn-O systems. At high sintering temperatures oxygen loss from the sample may also takes place, which changes the cation distribution in the spinel and the loss of one molecule of divalent oxygen will reduce two molecules of $Mn^{4+}$ to $Mn^{3+}$, hence decreases the hopping probability [25]. These spatial changes effectively reduce hopping probability, leads to an increase in activation energy of hopping, resistivity and *B*-value. Also the segregation or precipitation of impurities and additives at grain boundaries may form potential barriers, which also induce an increase in resistivity [3, 19]. Similar results were obtained in the case of $Al_2O_3$, $SiO_2$ and $Cr_2O_3$ addition in Ni–Mn–Co system [11–13].

Study of NTC thermistor samples by means of accelerated ageing provides a simple and direct method for evaluating the reliability features concerning the stability of the material. The results (Table 3) show an increase in reliability with increase in concentration of chromium. Although the presence of iron enhances the reliability of Ni–Mn–O system, its effect was found to be less compared to chromium. $Ni_{0.75}Mn_{(2.25-x-y)}Cr_xFe_yO_4$ ($x$=0 to 0.3 and $y$=0 to 0.3) compositions show a resistance drift ($\Delta R$) of less than +0.5%. This is an indication of excellent reliability of the material. The common industrial acceptance limit is ±1% resistance drift. A maximum reliability was obtained at a sintering temperature of 1200 °C, which is attributed to the single phase dense microstructure formation. Above 1200 °C the reliability shows a decline, caused by the segregation of NiO rich phase at grain boundaries. The segregation of impurities and charge compensation at grain boundaries influence thermistor performance and stability [1]. The Ni–Mn–Fe–Cr–O based systems shows a resistance drift of less than +0.5% compared to undoped sample (>+1.5%). Further studies regarding the factors affecting reliability of NTC ceramics is under progress in our laboratory.

## 4 Conclusion

In summary, the study reveals that a cubic spinel (space group *Fd* 3*m*) single-phase region exists over a wide compositional range for $Ni_{0.75}Mn_{(2.25-x-y)}Cr_xFe_yO_4$ ($x$=0 to 0.3 and $y$=0 to 0.3) when sintered in air at a temperature range of 1150 °C to 1200 °C and shows excellent NTC characteristics. The activation energy, resistivity and *B*-value of the thermistors increased with increasing $Cr_2O_3$ content and sintering temperature, and are attributed to the change in cation distribution originated from the clustering of $Mn^{3+}$ ions in octahedral sites and also by the dilution effect of $Fe^{3+}$ and $Cr^{3+}$ substitution in the spinel lattice.

Furthermore, $Ni_{0.75}Mn_{(2.25-x-y)}Cr_xFe_yO_4$ system shows a resistance drift of less than +0.5% at an optimum sintering temperature of 1200 °C. The reliability of $Ni_{0.75}Mn_{(2.25-x-y)}Cr_xFe_yO_4$ system was significantly improved by the addition of chromium. The electrical and reliability characteristics of $Ni_{0.75}Mn_{(2.25-x-y)}Cr_xFe_yO_4$ system was found to be superior to Ni–Mn–O system and these materials are expected to have the potential for the development of highly reliable advanced thermal sensing devices.

## References


1. D.C. Hill, H.L. Tuller, in *Ceramic Materials for Electronics*, ed. by R.C. Buchanan (Marcel Dekker, New York, 1986), p. 249
2. E.D. Macklen, *Thermistors* (Electrochemical Publications Ltd., Scotland, 1979), p. 4
3. J.G. Fagan, V.R.W. Amarakoon, Am. Ceram. Soc. Bull. **72**, 70 (1993)
4. G. Lavenuta, Sensors, **14**, 46 (1997)
5. S. Fritsch, J. Sarrias, M. Brieu, J.J. Coudere, J.L. Baudour, E. Snoeck, A. Rousset, Solid State Ionics, **109**, 229 (1998)
6. C. Drouet, C. Laberty, J.L.G. Fierro, P. Alphonse, A. Rousset, Int. J. Inorg. Mater. **2**, 419 (2000)
7. M. Hosseini, B. Yasaei, Ceram. Int. **24**, 543 (1998)
8. Y. Abe, T. Meguro, T. Yokoyama, T. Morita, J. Tatami, K. Komeya, J. Ceram. Process. Res. **4**, 140 (2003)
9. E.S. Na, U.G. Paik, S.C. Choi, J. Ceram. Process. Res. **2**, 31 (2001)
10. K. Park, D.Y. Bang, J.G. Kim, J.Y. Kim, C.H. Lee, B.H. Choi, J. Korean Phys. Soc. **41**, 251 (2002)
11. K. Park, I.H. Han, Mater. Sci. Eng. B. **119**, 55 (2005)
12. K. Park, J. Am. Ceram. Soc. **88**, 862 (2005)
13. K. Park, I.H. Han, J. Electroceram. **17**, 1069 (2006)
14. Justin M. Varghese, A. Seema, K.R. Dayas, Mater. Sci. Eng. B. **149**, 47 (2008)
15. Y.V. Golikov, V.F. Balakirev, J. Phys. Chem. Solids. **49**, 329 (1998)
16. F. Golestani-Fard, S. Azimi, K.J.D. Mackenzie, J. Mater. Sci. **22**, 2847 (1987)
17. M. Hirai, H. Yamamoto, J. Mass. Spectrom. **46**, 296 (1998)
18. J.J. Cooper, Ceram. Eng. Sci. Proc. **12**, 133 (1991)
19. O. Bodak, L. Akselrud, P. Demchenko, B. Kotur, O. Mrooz, I. Hadzaman, O. Shpotyuk, F. Aldinger, H. Seifert, S. Volkov, V. Pekhnyo, J. Alloys Compd. **347**, 14 (2002)
20. G.D.C. Cste de Gyorgyfalva, I.M. Reaney, J. Mater. Res. **18**, 1301 (2003)
21. G.D.C. Cste de Gyorgyfalva, I.M. Reaney, J. Eur. Ceram. Soc. **21**, 2145 (2001)
22. W.D. Kingery, H.K. Bowen, D.R. Uhlmann, *Introduction to Ceramics*, 2nd edn. (John Wiley & Sons, Singapore, 2004), p. 197
23. H. Yamamoto, A. Shibata, K. Hajime, F. Takao, K. Sugisawa, Y. Niwatsukino, H. Shishiba, S. Takeda, *Proceedings of the Ninth IEEE International Symposium on Applications of Ferroelectrics* (The Pennsylvania State University, Pennsylvania, 1994), p. 735
24. S.A. Kanade, V. Puri, Mater. Lett. **60**, 1428 (2006)
25. E.D. Macklen, J. Phys. Chem. Solids. **47**, 1073 (1986)